Supporting Information for

Nd^{3+}-Sensitized Upconversion Nanophosphors: Efficient *in vivo* Bioimaging Probes with Minimized Heating Effect

Ye-Fu Wang, Gao-Yuan Liu, Ling-Dong Sun,* Jia-Wen Xiao, Jia-Cai Zhou, and Chun-Hua Yan*

Beijing National Laboratory for Molecular Sciences, State Key Laboratory of Rare Earth Materials Chemistry and Applications & PKU-HKU Joint Laboratory in Rare Earth Materials and Bioinorganic Chemistry, College of Chemistry and Molecular Engineering, Peking University, Beijing 100871, China.

E-mail: sun@pku.edu.cn (L. D. Sun), yan@pku.edu.cn (C. H. Yan)

Experimental Details

Sample composition. Detailed compositions of samples mentioned in this work are listed below:

$NaGdF_4$:Yb,Er@$NaGdF_4$:Nd,Yb (Er@Nd)	β-$NaGd_{0.78}F_4$:$Yb_{0.20}$,$Er_{0.02}$@β-$NaGd_{0.80}F_4$:$Nd_{0.10}$,$Yb_{0.10}$
$NaGdF_4$:Yb,Er@$NaGdF_4$:X,Yb (Er@X)	β-$NaGd_{0.78}F_4$:$Yb_{0.20}$,$Er_{0.02}$@β-$NaGd_{0.80}F_4$:$X_{0.10}$,$Yb_{0.10}$
$NaGdF_4$:Nd,Er	β-$NaGd_{0.78}F_4$:$Nd_{0.20}$,$Er_{0.02}$
$NaGdF_4$:Nd,Yb,Er	β-$NaGd_{0.78}F_4$:$Nd_{0.10}$,$Yb_{0.10}$,$Er_{0.02}$
$NaGdF_4$:Yb,Tm@$NaGdF_4$:Nd,Yb (Tm@Nd)	β-$NaGd_{0.598}F_4$:$Yb_{0.400}$,$Tm_{0.002}$@β-$NaGd_{0.80}F_4$:$Nd_{0.10}$,$Yb_{0.10}$

Absorption of water and tissues. The absorption spectrum of water is plotted based on the data reported in the literature.[S1] The tissue absorption spectrum is calculated with the formula reported:[S2]

$$\mu_a(\lambda) = S_B(x\,\mu_{a,Hb}(\lambda) + (1\text{-}x)\,\mu_{a,HbO2}(\lambda)) + S\,w\mu_{a,W}(\lambda)$$

where $x = HbO_2/(HbO_2+Hb)$ and S_B and S_W are heuristic scaling factors for (Hb + HbO_2) and water, respectively, which are adjusted to match the absorption data available in the literature for each type of tissue. The S_B and S_W value involved in our calculation are listed below:

Tissue type	S_B	x	S_W
Adipose	0.0033	0.7	0.5
Muscle	0.07	0.8	0.5
Skin	0.06	0.75	0.5

Laser heating effect to water. For laser heating effect test, NPs dispersed in deionized water were first prepared based on a modified method according to the literature.[S3] NPs dispersed in cyclohexane (20 mg/mL, 5 mL) were first added to the DMF solution of $NOBF_4$ (10 mg/mL, 5 mL). After stirring for 2 hours, toluene was added to the mixture and the NPs were collected by centrifugation. Then the NPs were redispersed in 10 mL DMF and added with 30 mg polyacrylic acid (PAA, 25% saponicated). After stirring for 12 hours, acetone was added and NPs were collected by centrifugation. The NPs were then redispersed in deionized water, and the

concentration is determined by ICP-AES to be 5 mg/mL. Then 4.5 mL dispersion of NPs was transferred into 6-well plates and the temperature of the dispersion is monitored by a thermometer (TES 1310 Type-K, Changlong Co. Ltd.). The laser outlet was immobilized 1.5 cm above the water-air interface and the laser was at normal incidence. After the dispersion reached thermal equilibration with the environment (25 ℃), the laser was applied and the temperature of dispersion was recorded every 15 s. The heating effect test for pure water is carried out with the same protocol.

***In vitro* laser heating effect.** Human Embryonic Kidney (HEK) 293T cells were cultured at 37 ℃ and 5% CO_2 in Dulbecco's Modified Eagle Medium (DMEM) supplemented with 10% fetal bovine serum (FBS), 1% penicillin/streptomycin. HEK 293T cells were cultured in a 6-well plate (2×10^5 cells per well) and pre-incubated for 12 h. Then the cells were washed twice with PBS solutions, after then 4.5 mL PBS solution was added to the well and exposed to 808 nm or 980 nm laser (about 400 mW/cm^2) to study the laser induced cell damage effect. After irradiation, the cells were washed twice with PBS solutions. For live-dead assay, the cell was stained by mixed dye solution (Calcein acetoxymethyl ester, CAM, and Propidium Iodide, PI). CAM is originally non-fluorescent and could penetrate membrane of live cell. In live cells, CAM hydrolyzes with intracellular esterases and converts to calcein with strongly green fluorescence. PI is an ethidium bromide derivative and intercalates into double-stranded nucleic acids. When it enters damaged membrane and stains dead cell nucleus, it emits red fluorescence under the excitation of 543 nm. 1 mL dye solution was added into each well, and after 10 min of staining the cells were rinsed by PBS twice. Fluorescence images were taken by Nikon A1R fluorescence microscope. Fluorescence signal from CAM was collected from the FITC channel (with a 465−495 nm excitation bandpass filter, and a 515−555 nm emission bandpass filter). Fluorescence signal from PI was collected from the TRITC channel (with a 528−552 nm excitation bandpass filter, and a 578−632 nm emission bandpass filter).

References

S1. Prahl, S. Optical Properties Spectra, http://omlc.ogi.edu/spectra/index.html (accessed Oct. 17, 2012).

S2. Alexandrakis, G.; Rannou, F. R.; Chatziioannou, A. F. Tomographic Bioluminescence Imaging by Use of a Combined Optical-PET (OPET) System: a Computer Simulation Feasibility Study. *Phys. Med. Biol.* **2005**, *50*, 4225-4241.

S3. Dong, A.; Ye, X.; Chen, J.; Kang, Y.; Gordon, T.; Kikkawa, J. M.; Murray, C. B. A Generalized Ligand-Exchange Strategy Enabling Sequential Surface Functionalization of Colloidal Nanocrystals *J. Am. Chem. Soc.* **2011**, *133*, 998-1006.

Additional Figures

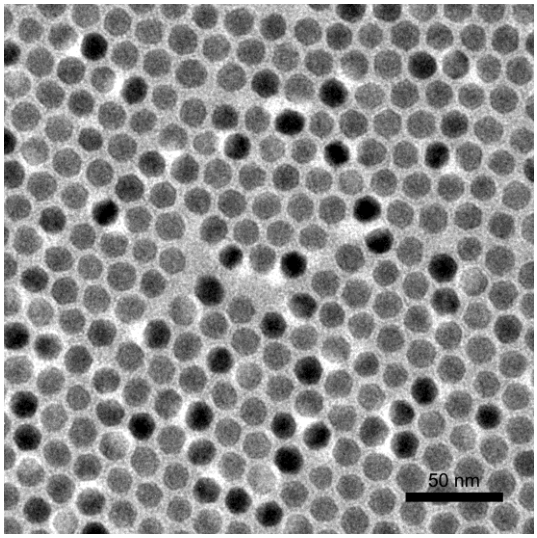

Figure S1. TEM image of the as-prepared $NaGdF_4$:Yb,Er NPs.

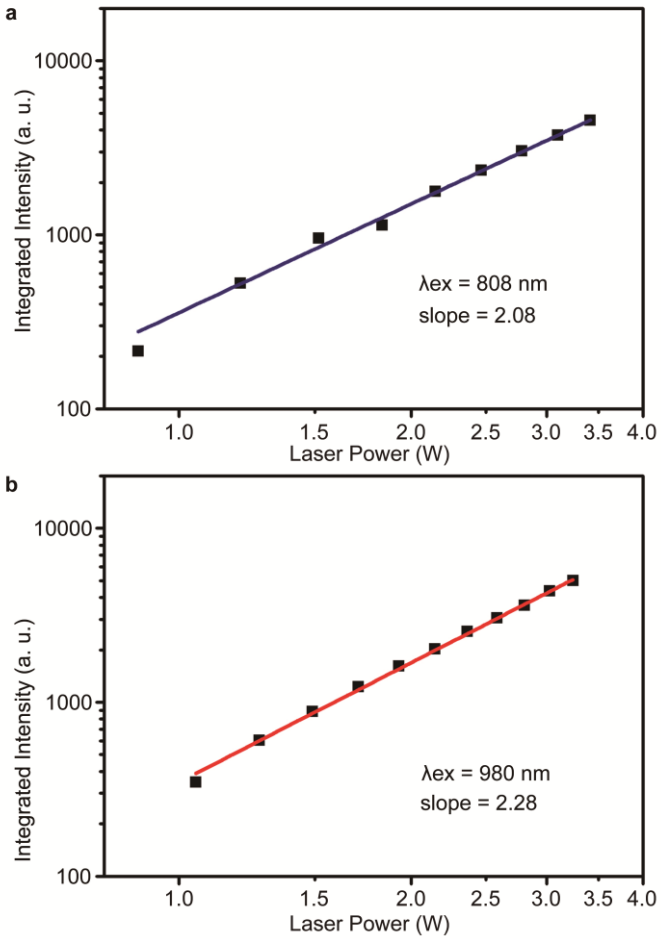

Figure S2. Dependence of integrated emission intensity on excitation power for (a) 808 nm laser and (b) 980 nm laser for Er@Nd NPs. The intensity is integrated from 500 nm to 570 nm for the $^2H_{11/2}$, $^4S_{3/2}\rightarrow{}^4I_{15/2}$ transitions of Er^{3+}. The value of slope is obtained by linear fitting of log (Intensity) to log (laser power).

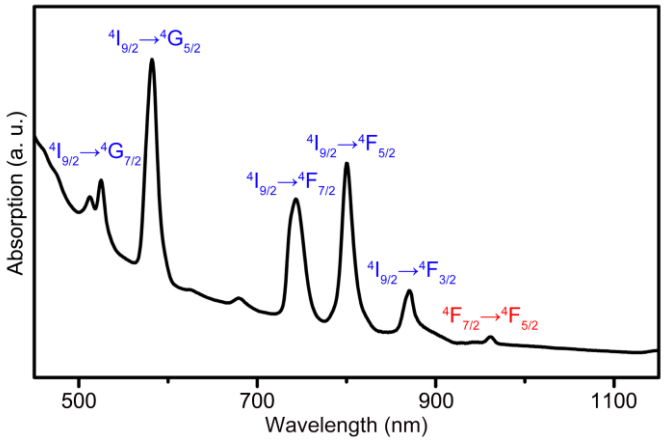

Figure S3. Absorption spectrum of Er@Nd NPs dispersed in cyclohexane. Transitions from Nd^{3+} and Yb^{3+} are denoted in blue and red, respectively.

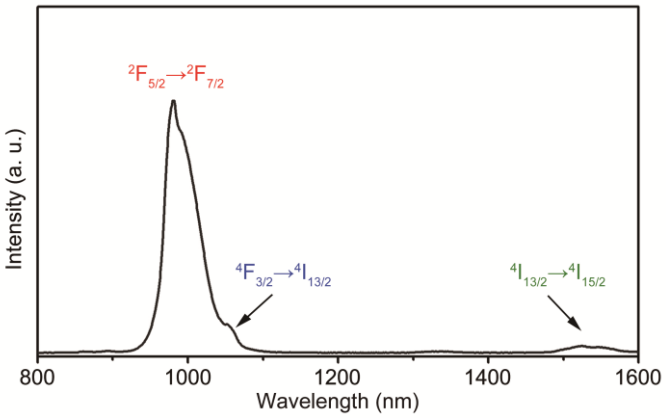

Figure S4. NIR emission spectrum of Er@Nd NPs. Transitions from Yb^{3+}, Nd^{3+} and Er^{3+} are denoted in red, blue and green, respectively.

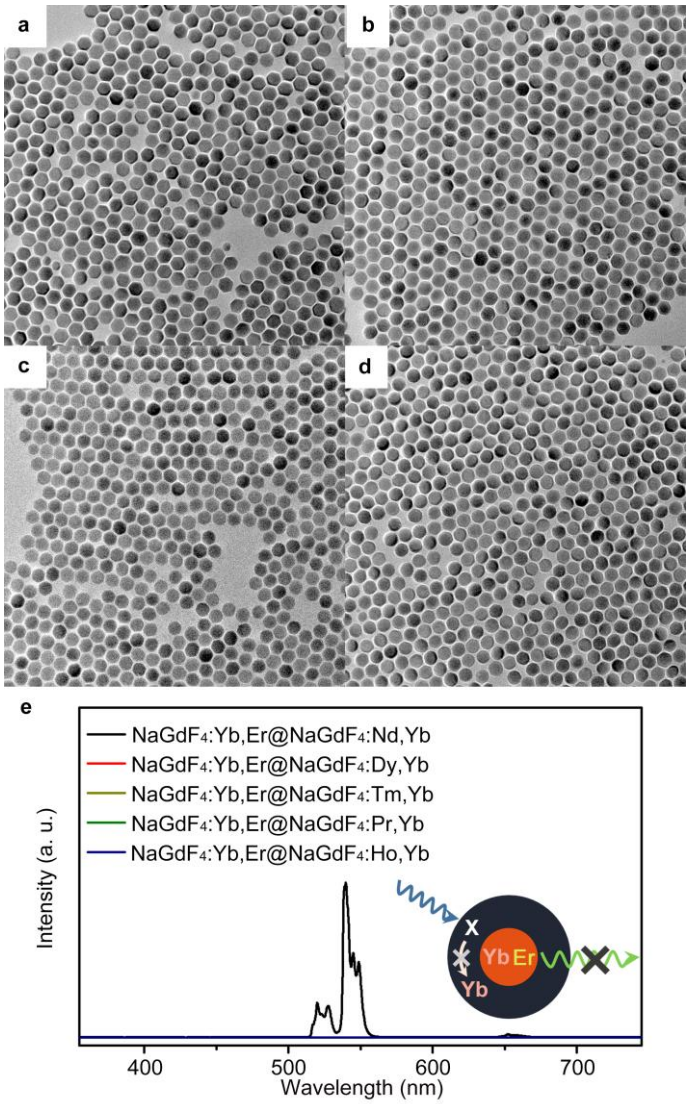

Figure S5. (a-d) TEM images of Er@X NPs, for (a) X = Dy, (b) X = Tm, (c) X = Ho, (d) X = Pr. (e) UC emission spectra of Er@Nd NPs and Er@X NPs under 808 nm laser excitation.

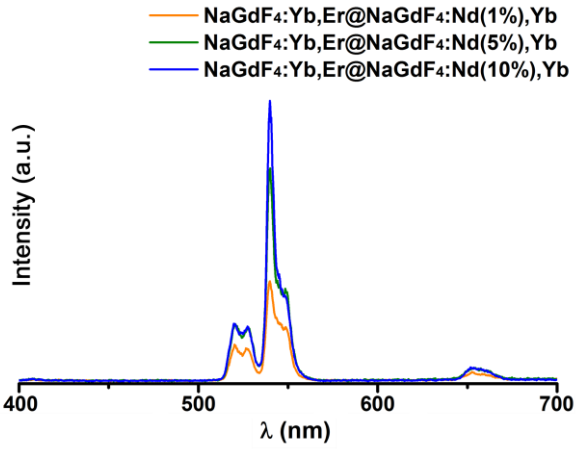

Figure S6. UC emission spectra of Er@Nd NPs with different Nd^{3+} doping concentration in the shell layer, under 808 nm laser excitation. The emission intensity is not proportional to the doping concentration, indicating the existence of Nd^{3+} self-quenching.

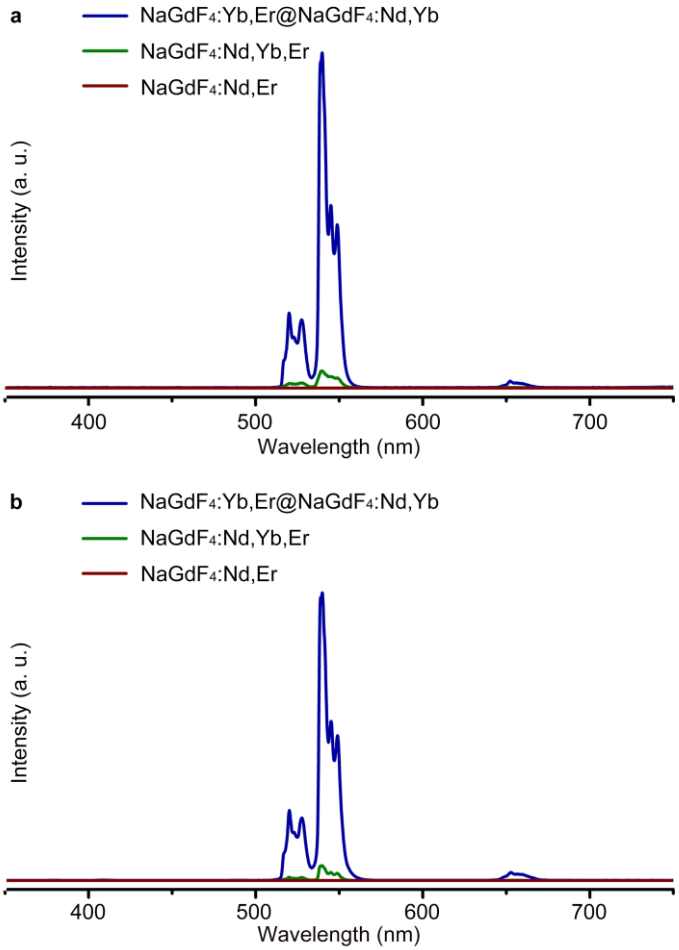

Figure S7. UC emission spectra of Er@Nd NPs, $NaGdF_4$:Nd,Er NPs and $NaGdF_4$:Nd,Yb,Er NPs under 808 nm laser excitation (a) and 980 nm laser excitation (b).

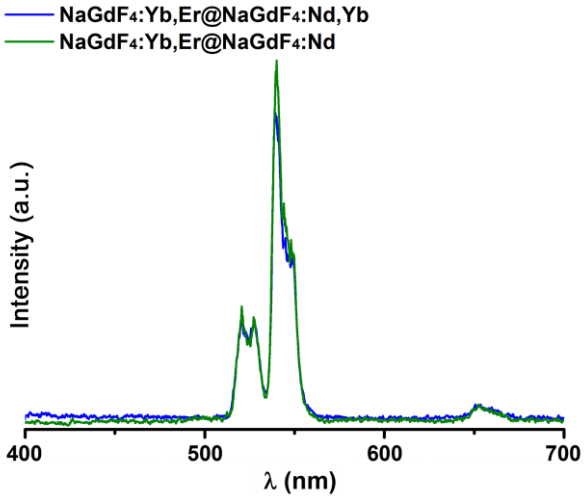

Figure S8. UC emission spectra of Er@Nd NPs and $NaGdF_4$:Yb,Er@Nd NPs with the same particle concentration. For the Nd^{3+} ions near the core, Yb^{3+} in shell would prolong the ET pathway and reduce the ET efficiency; on the other hand, for Nd^{3+} ions far from core, which could not well interact with Yb^{3+} in the core, Yb^{3+} in the shell benefit the ET from Nd^{3+} to Er^{3+} in the cores. As a result, in this case, similar emission intensity were found for the two types of NPs.

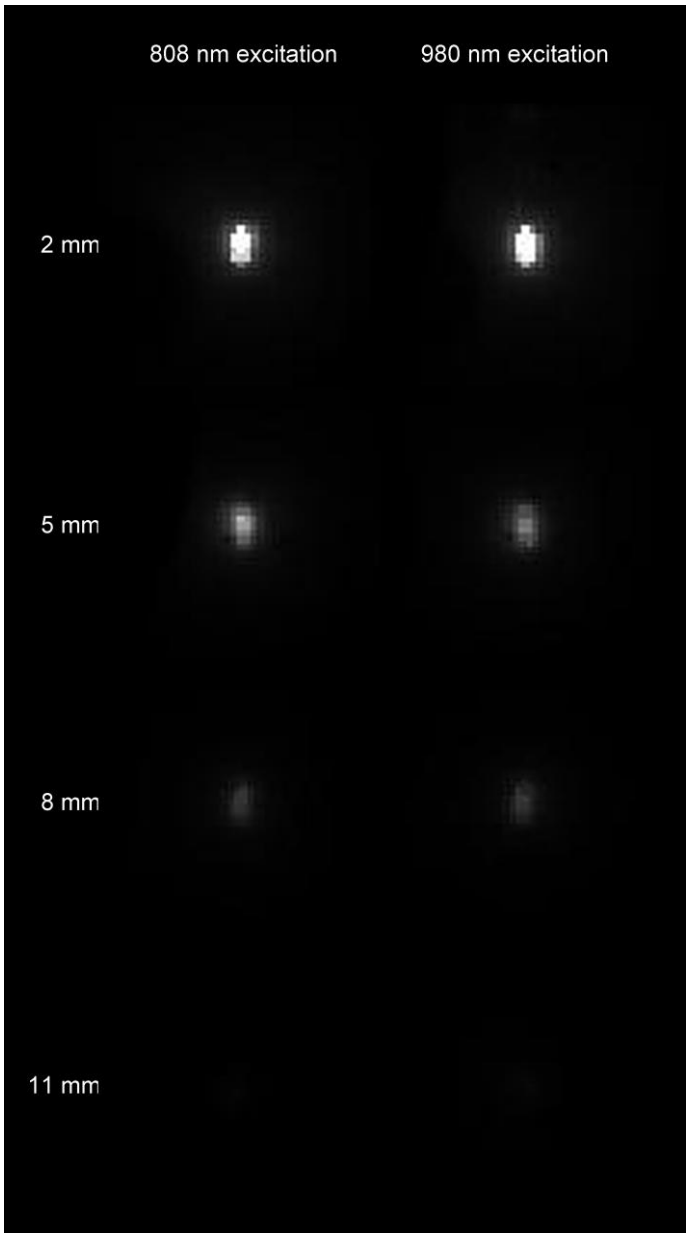

Figure S10. Tissue penetration depth tests carried out in agar phantom. The Er@Nd NPs sample sealed in a capillary was inserted into the phantom at different depths, and the UC images were then took by IVIS, under 808 nm laser (left) and 980 nm laser (right) irradiation, respectively. Both lasers were operated at power density of 200 mW/cm^2. Both bright spots with different excitation wavelengths disappear at the depth of 11 nm, implying a similar penetration depth limit for 808 nm laser and 980 nm laser excitation.

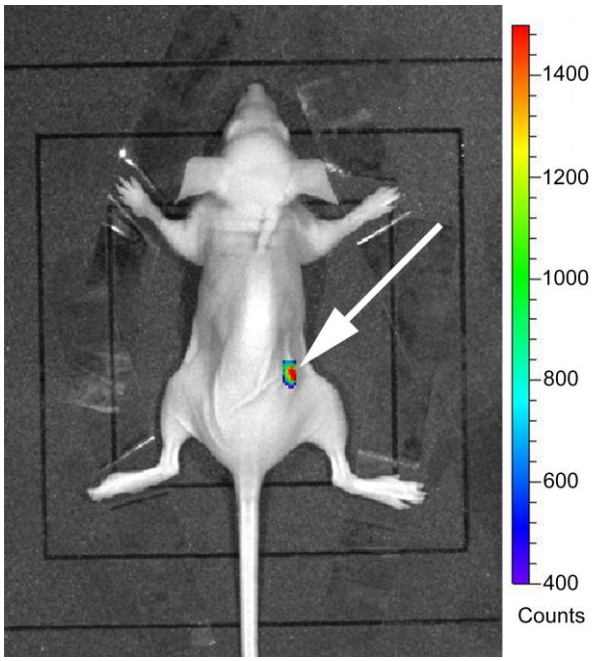

Figure S11. *In vivo* UC emission image of a BALB/c nude mice under 730 nm laser excitation (about 200 mW/cm^2), subcutaneously injected with Er@Nd NPs dispersed in water. Injection site is denoted as the white arrow.

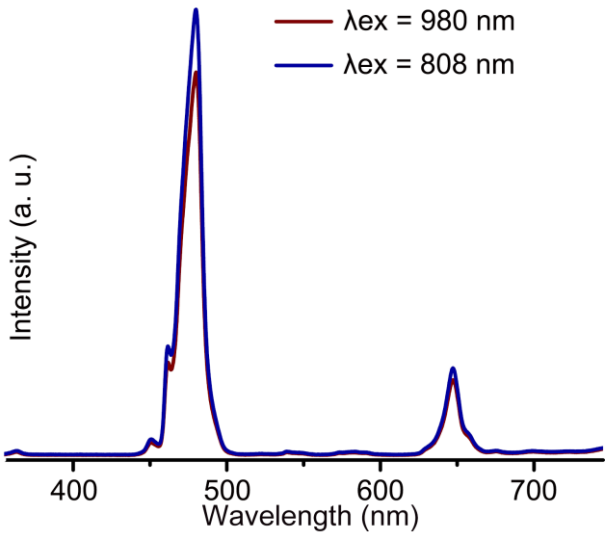

Figure S12. UC emission spectra of Tm@Nd NPs under 808 nm laser and 980 nm laser excitation, respectively.

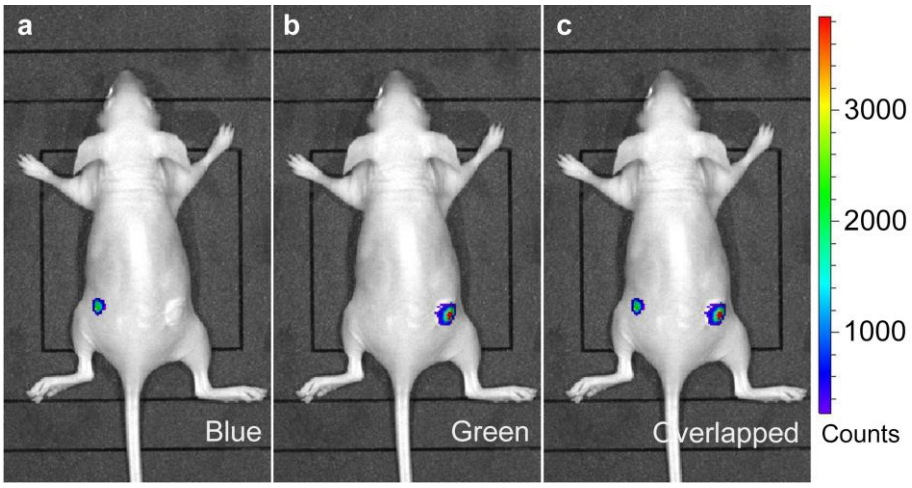

Figure S13. *In vivo* multicolor image from the blue (a) and green (b) channels under 808 nm excitation, the overlapped image shown in (c). The mouse was subcutaneously injected with Tm@Nd NPs and Er@Nd NPs at the left back and right back site, respectively.

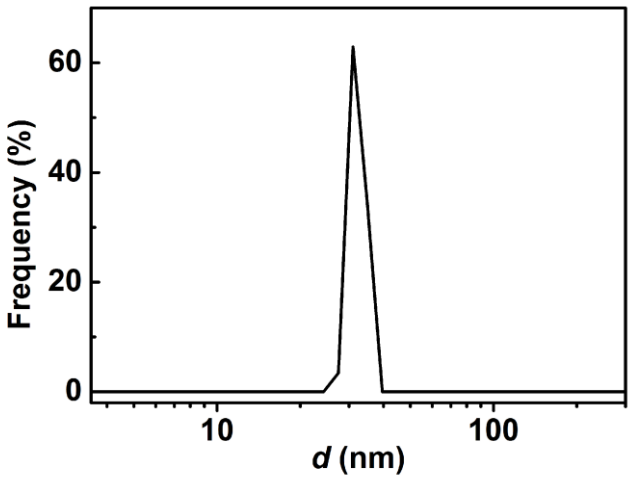

Figure S14. Hydrodynamic diameter distribution of Er@Nd NPs dispersed in water. The average hydrodynamic diameter is 30.0±2.0 nm.

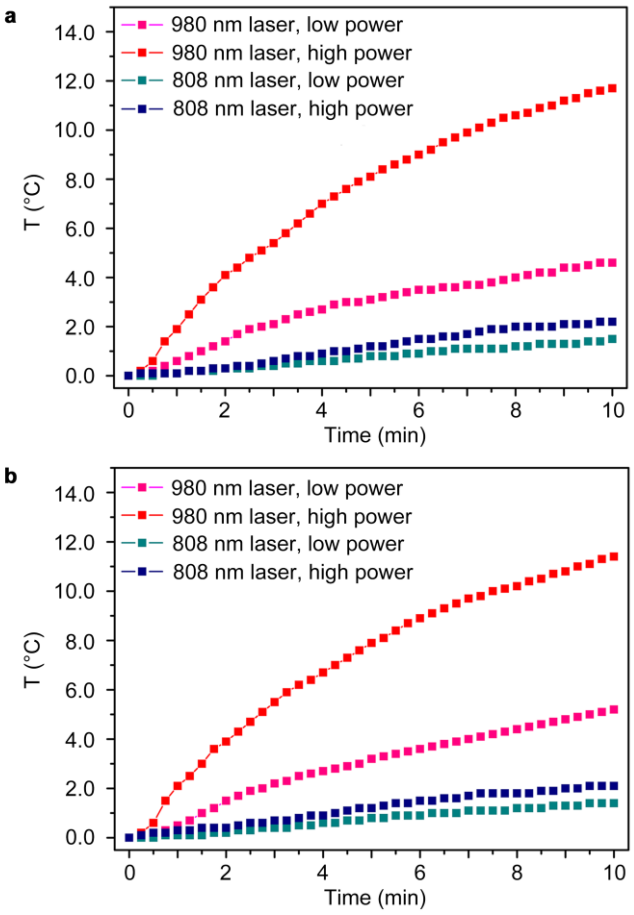

Figure S15. Temperature rise of (a) Er@Nd NPs dispersed in deionized water and (b) pure deionized water under 808 nm/980 nm laser irradiation at high (4.5 W) or low (1.5 W) power for 10 min irradiation.

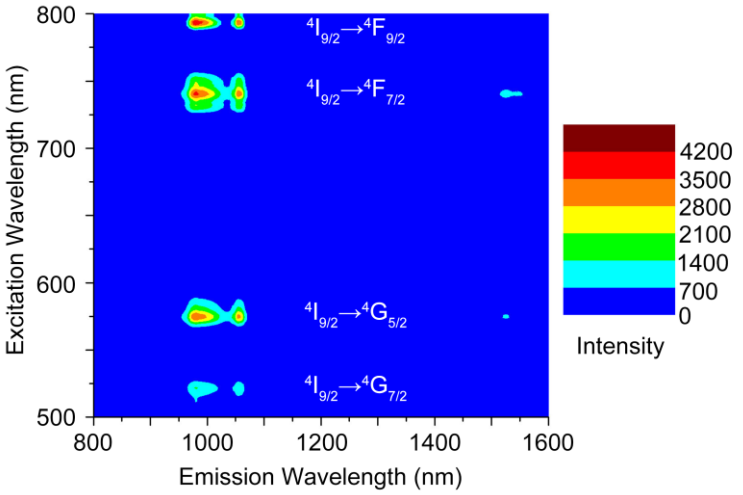

Figure S16. Three-dimensional excitation/emission spectrum in NIR region for Er@Nd NPs. The excitation transitions of Nd^{3+} are denoted.